Study of *PAPR* mitigation in OFDM-VLC system by SCMA codebook design*

YANG Ting, LI Ganggang, LIU Tao, WANG Ping, and WANG Zhao**

School of Telecommunications Engineering, Xidian University, Xi'an 710071, China

(Received 26 October 2023; Revised 3 April 2024)

Traditional orthogonal frequency division multiplexing (OFDM) based visible light communication (VLC) system is susceptible to high peak-to-average power ratio (*PAPR*), thus leading to low power efficiency. To address this issue, a sparse code multiple access (SCMA) codebook design method has been proposed to lower the *PAPR* of the clipping based OFDM-VLC system. Then, the codebooks of the high-dimension mother constellation (MC) and low-dimension MC are optimized, respectively. Specifically, for high-dimension MCs like T16-quadrature amplitude modulation (T16-QAM), the constellation points (CLPs) with higher transmit power are mapped to the CLPs with lower power. For low-dimension MCs like 4-pulse amplitude modulation (4-PAM), a contracted mapping method is proposed to reduce the power of the CLPs located on the real axis of the MC. Simulations show that the proposed method could achieve better *PAPR* performance for any value of the clipping ratio with only a slight bit error rate (*BER*) performance loss compared to the original codebook design. Besides, the smaller clipping ratio would induce better *PAPR* performance but worse *BER* performance. Moreover, the increasing number of iterations in the logarithm domain message passing algorithm (log-MPA) could improve the *BER* performance. This work will benefit the research and development of SCMA-OFDM-VLC systems.

Document code: A **Article ID:** 1673-1905(2024)09-0543-6

DOI https://doi.org/10.1007/s11801-024-3232-0

Visible light communication (VLC) technology has garnered significant attention as an important alternative to the existing radio frequency (RF) based wireless communications, particularly in the indoor scenarios with short communication ranges[1,2]. In VLC system, the orthogonal frequency division multiplexing (OFDM) scheme has been widely adopted for its high spectral efficiency[3]. Besides, the sparse code multiple access (SCMA) technique, which utilizes various codebooks to distinguish different users, has been proposed as a promising multiple access technique for the fifth-generation (5G) and beyond[4]. Compared to the traditional orthogonal multiple access technologies, SCMA could provide up to 200% more connections with its superior codebook design[5,6]. To further exploit the limited spectrum resource of the light-emitting diode (LED), the SCMA scheme has been introduced into VLC systems by some groups[1,7]. Unfortunately, the SCMA-OFDM-VLC system suffers from the inherent high peak-to-average power ratio (*PAPR*) of OFDM signals, causing the high-power amplifier (HPA) of the transmitter to work at saturation, therefore producing both in-band and out-of-band distortion[8]. To solve this problem, the simplest approach is to use the clipping technique[8-12]. Ref.[9] proposed a novel clipping-piecewise linear companding scheme to address the high clipping noise and *PAPR* in the OFDM-VLC system. Ref.[11] presented the μ-law nonlinear companding transform (μ-NCT) with modified recoverable upper-clipping (μ-NCT+MoRoC) model to reduce the *PAPR*. Actually, from the perspective of codebook design, the *PAPR* could be reduced if the SCMA codebook is designed properly[13], which has not been reported up to now for the SCMA-OFDM-VLC system, to the best of our knowledge. To this end, a novel codebook design method has been proposed in this work to mitigate the *PAPR* of the clipping based SCMA-OFDM-VLC system.

The contributions of this work could be summarized as follows. For the high-dimension mother constellation (MC), the constellation points (CLPs) with higher transmit power are mapped into the points with lower power to reduce the number of the high-power CLPs. For the low-dimension MC, the contracted mapping factor is proposed to reduce the power of those CLPs located on the real axis and further suppress the *PAPR*. Furthermore, simulation results are presented to evaluate both *PAPR* and bit error rate (*BER*) performances, where the validity of the proposed SCMA codebook design method is

* This work has been supported by the National Natural Science Foundation of China (No.62071365), and the Key Research and Development Program of Shaanxi Province (No.2017ZDCXL-GY-06-02).

** WANG Ping is a professor at the School of Telecommunications Engineering, Xidian University. He received his Ph.D. degree in 2005 from Xidian University. His research interests are mainly in optical wireless communication and visible light communication. E-mail: pingwang@xidian.edu.cn

effectively verified.

The diagram of the downlink SCMA-OFDM-VLC system is presented in Fig.1. It is assumed that J=6 and K=4, which means the data of six users are transmitted by four physical resource blocks[14]. At the transmitter side, $\boldsymbol{X}=[X_1, X_2, ..., X_N]$ denotes the frequency-domain (FD) signal. N depicts the number of subcarriers. Through the N-point inverse fast Fourier transform (IFFT), the FD signal is converted to the time-domain (TD) signal, denoted by $\boldsymbol{x}=[x_1, x_2, ..., x_N]$ in the diagram. To mitigate the high *PAPR*, clipping technology is adopted here. Then the real and imaginary parts of the complex TD signal are directly separated after the IFFT processing. The signals with direct-current (DC) bias are expressed as $\widetilde{\mathrm{Re}}[\boldsymbol{x}]$ and $\widetilde{\mathrm{Im}}[\boldsymbol{x}]$, which are then rearranged alternately in the form of serial stream $\tilde{\boldsymbol{x}}=[\widetilde{\mathrm{Re}}[x_1], \widetilde{\mathrm{Im}}[x_1], \widetilde{\mathrm{Re}}[x_2], \widetilde{\mathrm{Im}}[x_2], ..., \widetilde{\mathrm{Re}}[x_N], \widetilde{\mathrm{Im}}[x_N]]$. The VLC channels are assumed to be unit vectors for simplicity, and the extension to the general VLC values is straightforward[4,15]. The additive white Gaussian noise (AWGN) is denoted by n with zero mean and variance σ_{W}^2. The received real signal is represented by $\tilde{\boldsymbol{y}}=[\tilde{y}_1, \tilde{y}_2, ..., \tilde{y}_{2N}]$, which is subsequently rearranged to the complex signal stream $\hat{\boldsymbol{y}}$, where $\hat{\boldsymbol{y}}=[\tilde{y}_1+\mathrm{i}\tilde{y}_2, \tilde{y}_3+\mathrm{i}\tilde{y}_4, ..., \tilde{y}_{2N-1}+\mathrm{i}\tilde{y}_{2N}]$. With the N-point FFT operation, the corresponding FD signal is obtained. To distinguish different users' signals, the logarithm domain message passing algorithm (log-MPA) is adopted to perform multi-user detection[16,17].

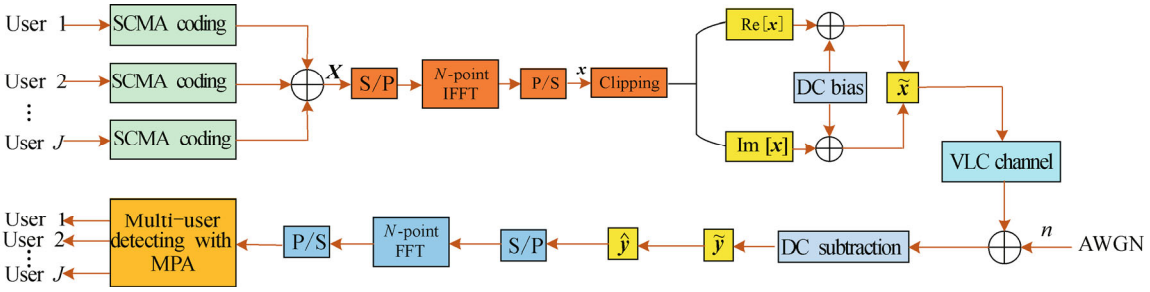

Fig.1 SCMA-OFDM-VLC system model

The N-point IFFT TD signal x_n can be given by

$$x_n=\frac{1}{\sqrt{N}}\sum_{k=1}^{N}X_k\mathrm{e}^{\mathrm{j}\frac{2\pi kn}{N}}, n=1,2,\ldots,N. \tag{1}$$

As a result, the *PAPR* can be expressed as

$$PAPR(x)=\frac{P_{\mathrm{p}}}{P_{\mathrm{a}}}=\frac{\max_{1\le n\le N}|x_n|^2}{\mathrm{E}\left[|x_n|^2\right]}, \tag{2}$$

where P_{p} and P_{a} represent the peak power and average power, respectively. $\mathrm{E}[\cdot]$ and $\max[\cdot]$ denote the mean and maximum operations, respectively.

Generally, to describe the probability that the *PAPR* achieves a higher value than a certain threshold, the complementary cumulative distribution function (*CCDF*) can be used and given by

$$CCDF(PAPR_0)=P\left[PAPR>PAPR_0\right], \tag{3}$$

where $PAPR_0$ represents the threshold.

The soft envelope limiter clipping model is considered[8], in which the clipped signal $\bar{x}_n$ is given by

$$\bar{x}_n=\begin{cases}x_n, & |x_n|\le A\\ A\cdot\mathrm{e}^{\mathrm{j}\angle x_n}, & |x_n|\ge A\end{cases}, \tag{4}$$

where A represents the clipping threshold. Consequently, the clipping ratio γ can be defined as $\gamma=\dfrac{A^2}{\mathrm{E}\left[|x_n|^2\right]}$.

The overall noise at the receiver consists of two parts, the clipping noise and the AWGN. The variance of the overall noise can be given by[8]

$$\sigma_{\mathrm{All}}^2=\alpha^{-2}\left(\sigma_{\mathrm{c}}^2+\sigma_{\mathrm{W}}^2\right), \tag{5}$$

where $\alpha=1-\mathrm{e}^{-\gamma}+\dfrac{\sqrt{\pi\gamma}}{2}\mathrm{erfc}(\sqrt{\gamma})$, is the attenuation factor. $\mathrm{erfc}(x)=\dfrac{2}{\sqrt{\pi}}\int_x^{\infty}\mathrm{e}^{-\eta^2}\mathrm{d}\eta$ depicts the complementary error function. $\sigma_{\mathrm{c}}^2=(1-\mathrm{e}^{-\gamma}-\alpha^2)\sigma_x^2$ is the variance of the clipping noise, where σ_x^2 represents the variance of the signal without clipping.

The SCMA encoding operation of the jth user can be expressed as $\boldsymbol{X}_j=f(\boldsymbol{b}_j)=\left[x_{1j}, x_{2j}, \ldots x_{Nj}\right]$, where $\boldsymbol{b}_j$ and $\boldsymbol{X}_j$ are the binary bit stream and SCMA codewords of jth user. f is the mapping relation between $\boldsymbol{b}_j$ and $\boldsymbol{X}_j$, which can be written as $f:\mathcal{B}^{\log_2 M}\to\chi$, where $\chi\subset\mathcal{C}^K$ with the cardinality $|\chi|=M$. $\mathcal{B}$ and $\mathcal{C}$ represent the sets of binary and complex numbers, respectively. The superimposed complex codeword can be given by $\boldsymbol{X}=\sum_{j=1}^{J}\boldsymbol{X}_j$.

Based on the above analysis, it can be known that the *PAPR* is significantly affected by the power of the CLPs in the MC. To this end, an SCMA codebook design method is presented to decrease the power of the CLPs with slight *BER* performance loss. For the high-dimension MC, the CLPs located in the corners are

mapped into other points with less power. For the low-dimension MC, the power of those CLPs located on the real axis of the MC is reduced. Without loss of generality, T16-quadrature amplitude modulation (T16-QAM) and 4-pulse amplitude modulation (4-PAM) are adopted to illustrate the high-dimension MC and low-dimension MC cases, respectively.

Fig.2 shows the projections on these two complex dimensions, which come from the MC of T16-QAM signaling, and each dimension corresponds to one certain resource block. In the projection of the dimension 1 (D1), there are four CLPs out of the unit circle corresponding to four codewords, i.e., 1100, 0000, 0011, and 1111, which have the largest amplitude among all the codewords. Similarly, in the projection of the dimension 2 (D2), there are also four CLPs out of the unit circle corresponding to four codewords, i.e., 1001, 0101, 0110, and 1010, which are allocated the highest power. Recall that high *PAPR* mainly results from those codewords with more power, and thus it is quite necessary to reduce the power of these codewords (corresponding to the red dots shown in Fig.2). To this end, for T16-QAM signaling constellation, the red CLPs are deleted from the MC and the corresponding codewords are mapped into other CLPs located inside the unit circle. The mapping transformation is characterized in Fig.3. It can be observed that there are four CLPs containing two different codewords in D1, i.e., {0110, 1100}, {1010, 0000}, {1001, 0011}, and {0101, 1111}. Similarly, there are also four CLPs containing two different codewords in D2, i.e., {1100, 1001}, {0000, 0101}, {0011, 0110}, and {1111, 1010}. According to the detecting policy of the log-MPA, the non-double-overlapping principle (NDOP) is presented that the overlapping codewords in a certain dimension should not be mapped into the same CLP in another dimension to avoid the detecting errors. Obviously, the designed constellation could satisfy the NDOP. In this work, the codebooks set (CS) corresponding to the original T16-QAM constellation is denoted by CS1-1, and the corresponding T16-QAM constellation is represented by MC1-1. Similarly, the CS corresponding to the proposed inward mapping 12-point constellation is expressed by CS1-2, and the corresponding 12-point constellation is denoted by MC1-2.

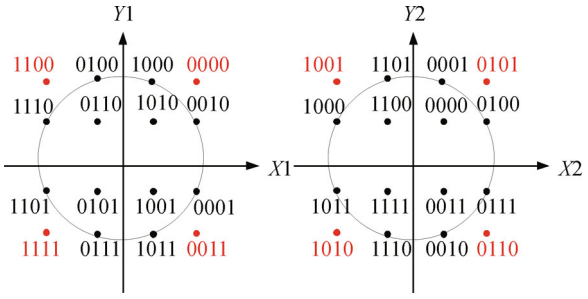

Fig.2 Projections on two complex dimensions of T16-QAM signaling constellation

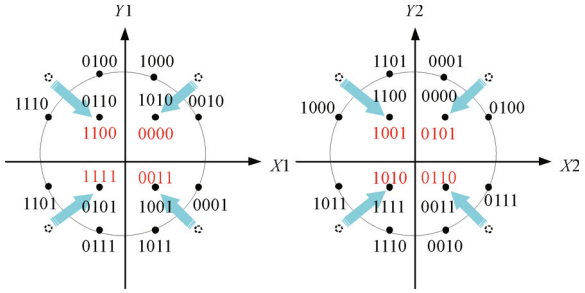

Fig.3 Inward mapping transformation of T16-QAM signaling constellation

Moreover, on the basis of the above mapping method, another strategy is proposed to improve the original MC (MC1-1). Fig.4 shows the detailed mapping strategy clearly, in which the codewords signed by red dots are mapped counterclockwise to the adjacent CLPs. The designed constellation also satisfies the NDOP. The CS corresponding to this 12-point constellation is represented by CS1-3, and the corresponding 12-point constellation is represented by MC1-3.

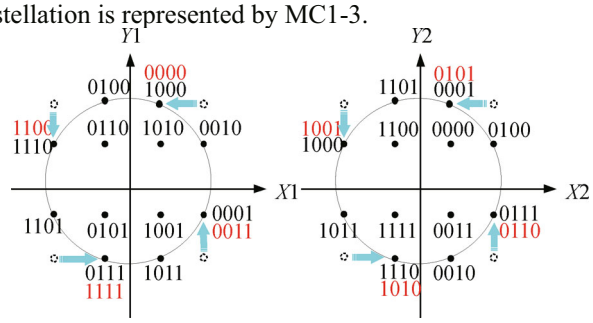

Fig.4 Counterclockwise mapping transformation of T16-QAM signaling constellation

For the low-dimension MC like 4-PAM, the delete operation is unrealistic due to the limited number of CLPs. Therefore, a contracted mapping method is proposed. Specifically,

- Generate the MC.
- Determine the sparse matrix $\boldsymbol{V}_j$ of jth user according to the factor matrix $\boldsymbol{F}$.
- Determine the operating matrix $\boldsymbol{\Delta}_j$ and the final codebook $\boldsymbol{C}_j$ of jth user, on the basis of the relationship $\boldsymbol{C}_j = \boldsymbol{V}_j(\boldsymbol{\Delta}_j)\boldsymbol{C}_{\mathrm{MC}}$.

The MC of 4-PAM signals are depicted in Fig.5, which could be further expressed as

$$\mathbf{C}_{\mathrm{MC}} = \begin{bmatrix} -R_1 & -R_2 & R_2 & R_1 \\ R_2 & -R_1 & R_1 & -R_2 \end{bmatrix}, \tag{6}$$

where $R_1 = |OA|$, $R_2 = |OB|$.

The factor matrix $\boldsymbol{F}$ for six users and four physical resource blocks can be given by[11]

$$\boldsymbol{F} = \begin{bmatrix} 0 & 1 & 1 & 0 & 1 & 0 \\ 1 & 0 & 1 & 0 & 0 & 1 \\ 0 & 1 & 0 & 1 & 0 & 1 \\ 1 & 0 & 0 & 1 & 1 & 0 \end{bmatrix}. \tag{7}$$

Meanwhile, on the basis of the factor matrix and $\boldsymbol{F} = \left[\mathrm{diag}(\boldsymbol{V}_1\boldsymbol{V}_1^{\mathrm{T}}), \mathrm{diag}(\boldsymbol{V}_2\boldsymbol{V}_2^{\mathrm{T}}), \cdots, \mathrm{diag}(\boldsymbol{V}_J\boldsymbol{V}_J^{\mathrm{T}})\right]$, it is explicitly to obtain the sparse matrix for each user.

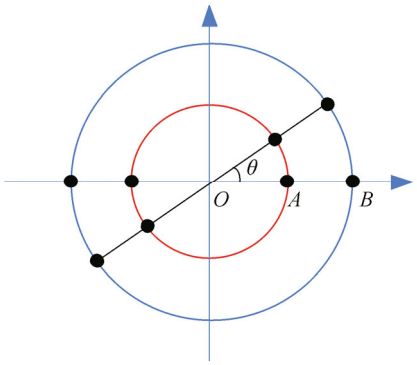

Fig.5 4-PAM constellation

The specific operating matrix Δ_j proposed in this work can be expressed as

$$\Delta_1=\begin{bmatrix} e^{i\theta_1} & 0 \\ 0 & \epsilon \end{bmatrix},\Delta_2=\begin{bmatrix} 0 & \epsilon \\ e^{i\theta_1} & 0 \end{bmatrix},\Delta_3=\begin{bmatrix} 0 & e^{i\theta_2} \\ e^{i\theta_3} & 0 \end{bmatrix},$$
$$\Delta_4=\begin{bmatrix} 0 & \epsilon \\ e^{i\theta_4} & 0 \end{bmatrix},\Delta_5=\begin{bmatrix} e^{i\theta_4} & 0 \\ 0 & e^{i\theta_2} \end{bmatrix},\Delta_6=\begin{bmatrix} 0 & \epsilon \\ e^{i\theta_3} & 0 \end{bmatrix}, \quad (8)$$

where ϵ represents the contracted mapping factor satisfying $0<\epsilon<1$. θ_1—θ_4 are the rotation angles. By utilizing the contracted mapping factor, the points located on the real axis of the MC could be mapped into the points located nearer the center of the circle. The CS corresponding to the original 4-PAM constellation is denoted by CS2-1, and the CS corresponding to the proposed constellation is represented by CS2-2.

Moreover, the computational complexity of this work is analyzed as follows. The OFDM-VLC system with SCMA technology contains N/K SCMA symbols in a frame, thus the decoding process of the SCMA-OFDM-VLC system requires $N/K*(3M^{d_f}Kd_f^2N_{iter}+2MKd_f)+2N\log_2 N$ additions, $N/K*(3M^{d_f}Kd_fN_{iter}+4MKd_f)+N\log_2 N$ multiplications, and $N/K*[M^{d_f}Kd_fN_{iter}+(N_v-2)MKd_fN_{iter}]$ comparisons, respectively, when the log-MPA is adopted for efficient decoding. M is the size of the user codebook, d_f denotes the degree of the function nodes, and N_v represents the degree of the variable nodes[17].

In this paper, the number of subcarriers and OFDM symbols are set to 512 and 3×10^5, respectively. The *CCDF* curves of the *PAPR* for the original T16-QAM CS and the proposed CSs with different clipping ratios are presented in Fig.6. It is evident that for any value of the clipping ratio, both proposed strategies exhibit better *PAPR* performance compared to the original scheme. However, as the clipping ratio increases, the enhancement in *PAPR* performance becomes limited due to the reduced differences between the clipped and original TD signals.

Fig.7 demonstrates the *BER* performance of the system operating under the original T16-QAM CS and our proposed CSs. Expectedly, the *BER* values would decrease with the increasing signal-to-noise ratio (*SNR*). The schemes with the proposed CSs show worse *BER* performances compared to the CS1-1 (the original T16-QAM CS) for any value of the clipping ratio. This is because after inward mapping or counterclockwise mapping operations, the minimum Euclidean distance of MC1-2 and MC1-3 would become smaller than that of MC1-1, which may cause unexpected detecting error. Specifically, the CS1-3 could provide better *BER* performance than that of CS1-2. Moreover, as the clipping ratio increases, the *BER* performance of this system would get better for these three CSs.

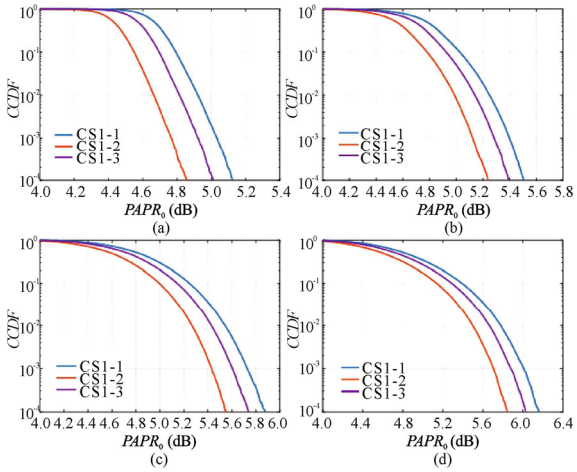

Fig.6 *PAPR* performance of the SCMA-OFDM-VLC system for T16-QAM with different values of the clipping ratio: (a) *γ*=4; (b) *γ*=5; (c) *γ*=6; (d) *γ*=7

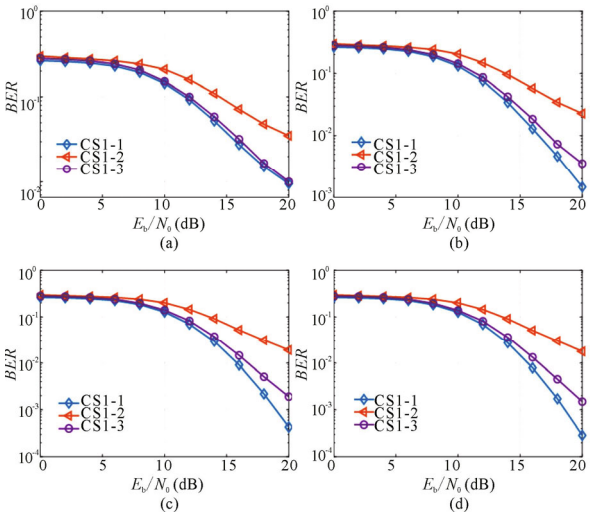

Fig.7 *BER* performance of the SCMA-OFDM-VLC system for T16-QAM with different values of the clipping ratio: (a) *γ*=4; (b) *γ*=5; (c) *γ*=6; (d) *γ*=7

The *CCDF* curves of the *PAPR* for the original 4-PAM CS and the proposed CSs with different clipping ratios and contracted mapping factors are illustrated in Fig.8. It can be observed that for any value of the clipping ratio, the proposed MC mapping scheme could significantly enhance the *PAPR* performance of this system compared to CS2-1. Specifically, the *PAPR* would become smaller

with the decreasing contracted mapping factors. Moreover, with the increase of the clipping ratio, the *PAPR* performance would get worse as expected.

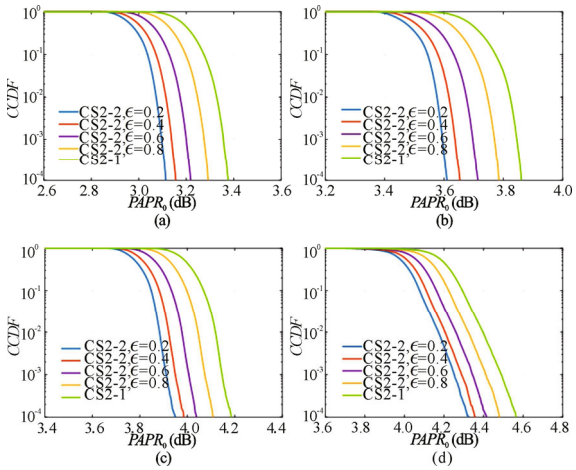

Fig.8 *PAPR* performance of the SCMA-OFDM-VLC system for 4-PAM with different values of the clipping ratio: (a) γ=1; (b) γ=2; (c) γ=3; (d) γ=4

Fig.9 shows the *BER* performance of this SCMA-OFDM-VLC system operating under the original 4-PAM CS and the proposed CSs with different clipping ratios and contracted mapping factors. It is evident that the *BER* would increase as the contracted mapping factor decreases. Recall that the *PAPR* performance could be efficiently enhanced with the contracted mapping factor being smaller as demonstrated in Fig.8. Therefore, there exists a trade-off between the *PAPR* and *BER* performances when choosing an appropriate contracted mapping factor. It is observed that the *BER* sharply increases when the contracted mapping factor decreases from 0.4 to 0.2. Besides, the *BER* performance would become better with the increasing clipping ratios.

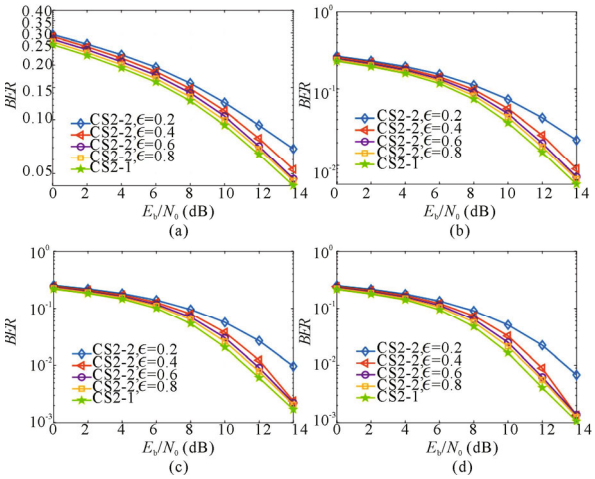

Fig.9 *BER* performance of the SCMA-OFDM-VLC system for 4-PAM with different values of the clipping ratio: (a) γ=1; (b) γ=2; (c) γ=3; (d) γ=4

The *BER* performance of this SCMA-OFDM-VLC system with T16-QAM and 4-PAM versus the number of iterations for log-MPA is depicted in Fig.10. For T16-QAM, the clipping ratio is 6 and the CS1-3 is adopted. As can be observed, the *BER* values would decrease with the increasing number of iterations in log-MPA. However, the improvement of the *BER* performance would not be obvious if the number of iterations for log-MPA is beyond 4, which means that there exists a potential bottleneck. For 4-PAM scheme, the clipping ratio is set to 3, and the contracted mapping factor for CS2-2 is set to 0.4. Similarly, the *BER* performance can be significantly improved as the number of iterations increases. Nevertheless, the *BER* performance improvement would not be pronounced if the number of iterations is larger than 3, which means that there also exists a potential bottleneck in improving the *BER* performance by increasing the number of iterations.

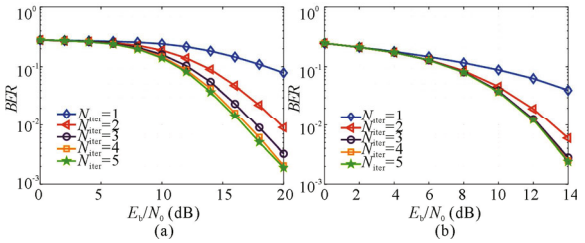

Fig.10 *BER* performance of the SCMA-OFDM-VLC system for (a) T16-QAM (CS1-3, γ=6) and (b) 4-PAM (CS2-2, ϵ = 0.4 , γ=3) with different numbers of iterations for log-MPA decoding operation

In this work, an SCMA codebook design method was proposed to reduce the *PAPR* of the clipping based SCMA-OFDM-VLC system. Different mapping strategies were presented for the high-dimension MC and low-dimension MC, respectively. Particularly, for the high-dimension MCs like T16-QAM, the CLPs with higher power in the original MC were mapped inward or counterclockwise to other CLPs with lower power. For the low-dimension MCs like 4-PAM, a contracted mapping method was proposed to reduce the power of the CLPs located on the real axis, thereby decreasing the overall *PAPR*. The effects of different CSs along with diverse parameters on the *PAPR* and *BER* performances of this SCMA-OFDM-VLC system were then simulated and compared. Results showed that the proposed SCMA codebook design method could significantly improve the *PAPR* performance with only a slight increase in *BER*. Meanwhile, with the growing of the clipping ratio, the *PAPR* performance would be degraded and the *BER* performance would be improved. Furthermore, the *BER* performance could be efficiently improved with the increasing number of iterations in the log-MPA decoding operation, while for a given *SNR*, the *BER* value would keep almost a constant as the number of iterations increases.

Ethics declarations

Conflicts of interest

The authors declare no conflict of interest.

References

[1] LIN B, LAI Q, LUO J, et al. A deep neural networks based demodulator for PD-SCMA-VLC[J]. Optics communications, 2023, 532: 129256.

[2] WANG D, LI C, CHE Y. Tunnel visible light communication system utilizing frequency domain pre-equalization technique[J]. Optoelectronics letters, 2022, 18(8): 484-488.

[3] NIU S, WANG P, CHI S, et al. Enhanced optical OFDM/OQAM for visible light communication systems[J]. IEEE wireless communications letters, 2021, 10(3): 614-618.

[4] CHATURVEDI S, ANWAR D N, BOHARA V A, et al. Low-complexity codebook design for SCMA-based visible light communication[J]. IEEE open journal of the communications society, 2022, 3: 106-118.

[5] LUO Q, LIU Z, CHEN G, et al. Enhancing signal space diversity for SCMA over Rayleigh fading channels[J]. IEEE transactions on wireless communications, 2023.

[6] MIUCCIO L, PANNO D, RIOLO S. A flexible encoding/decoding procedure for 6G SCMA wireless networks via adversarial machine learning techniques[J]. IEEE transactions on vehicular technology, 2023, 72(3): 3288-3303.

[7] AN J, CHUNG W. Single-LED multichannel optical transmission with SCMA for long range health information monitoring[J]. Journal of lightwave technology, 2018, 36(23): 5470-5480.

[8] YANG L, LIN X, MA X, et al. Clipping noise-aided message passing algorithm for SCMA-OFDM system[J]. IEEE communications letters, 2018, 22(10): 2156-2159.

[9] WANG Z, WANG P, NAN X, et al. PAPR reduction by combining clipping and piecewise linear companding for OFDM-based VLC systems[J]. Optical engineering, 2021, 60(6): 066105.

[10] LIAN J, BRANDT-PEARCE M. Clipping-enhanced optical OFDM for visible light communication systems[J]. Journal of lightwave technology, 2019, 37(13): 3324-3332.

[11] RAMAZAN M, AMCA H, RIZANER A, et al. A novel μ-law nonlinear companding with modified recoverable upper clipping method for PAPR reduction in ACO-OFDM VLC systems[J]. Optik, 2023, 282.

[12] HOU Y, LV J, ZHANG L, et al. Reduction of peak-to-average power ratio in visible light communication system using clipping and normalized μ-law companding[J]. Journal of optoelectronics·laser, 2022, 33(11): 1192-1200. (in Chinese)

[13] CHEN Y M, WANG P H, CHENG C S, et al. A joint design of SCMA codebook and PTS-based PAPR reduction for downlink OFDM scheme[J]. IEEE transactions on vehicular technology, 2022, 71(11): 11936-11948.

[14] MU H, MA Z, ALHAJI M, et al. A fixed low complexity message pass algorithm detector for up-link SCMA system[J]. IEEE wireless communications letters, 2015, 4(6): 585-588.

[15] GAO Q, HU S, GONG C, et al. Distance-range-oriented constellation design for VLC-SCMA downlink with signal-dependent noise[J]. IEEE communications letters, 2019, 23(3): 434-437.

[16] ZHANG S, XU X, LU L, et al. Sparse code multiple access: an energy efficient uplink approach for 5G wireless systems[C]//Proceedings of 2014 IEEE Global Communications Conference, December 8-12, 2014, Austin, TX, USA. New York: IEEE, 2014: 4782-4787.

[17] LIU J, WU G, LI S, et al. On fixed-point implementation of log-MPA for SCMA signals[J]. IEEE wireless communications letters, 2016, 5(3): 324-327.